Design of SIW-Based Multi-Aperture Couplers Using Ray Tracing Method

Zheng Liu, *Student Member, IEEE*, and Gaobiao Xiao, *Member, IEEE*

***Abstract*— In this paper, a simplified ray tracing method is used to approximately predict the coupling characteristics of H-plane multi-aperture substrate integrated waveguide (SIW) couplers. The output powers of the output ports are calculated with the reflection and the transmission coefficients at the coupling windows. The ray tracing method provides a simple and efficient way to determine the initial values for the geometrical parameters of SIW-based multi-aperture couplers. From these initial values, the structures of the couplers can be quickly optimized with less iterations, so that the design efficiency can be greatly improved. In order to get high isolation, a criterion is introduced to prevent exciting higher order propagating Floquet modes in the SIWs. Three examples of multi-aperture couplers are designed with our approach. The measured results agree well with the simulated results and the ones predicted using the ray tracing method.**

***Index Terms*— Directional coupler, Floquet theorem, isolation, ray tracing method, substrate integrated waveguide (SIW).**

I. Introduction

WAVEGUIDE couplers are the key components that have been widely employed in microwave- and millimeter-wave communication systems. However, their bulky size and nonplanar structures have restricted their application in microwave integrated circuits (MICs). Recently, couplers based on substrate integrated waveguide (SIW) technology are considered as promising candidates for MICs due to their wide bandwidth, low cost, and easy integration capabilities with other planar circuits [1]–[5].

The coupling mechanism of SIW-based couplers can be divided into broad-wall and narrow-wall coupling. Couplers realized by broad-wall coupling generally achieve better broadband performance, while narrow-wall couplers are especially useful for high-power applications [6]. In this paper, we focus on the H-plane SIW couplers. Some SIW-based couplers with large single coupling apertures are proposed in [7]–[14]. If SIW couplers are designed with multiple coupling sections, the extra degrees of freedom can be used to improve the operating bandwidth and optimize the coupling coefficients between output ports [15]. Therefore, some SIW-based multi-aperture couplers have been published in [16]–[19]. SIW-based couplers are usually designed by simulating and optimizing the entire component with commercial electromagnetic (EM) simulators, which may consume a lot of CPU time and memory, especially for multi-aperture couplers. As shown in [16], [19], and [20], the coupling characteristics can be approximately estimated when the transmission coefficients of the coupling windows within the couplers are known. The coupling windows are usually composed of finite-length periodic via arrays. For an infinite grid array consisting of metallic vias, the transmission coefficient can be calculated with some closed-form formulas [20]–[22]. However, these formulas are applicable only when the size of metallic vias and the spacing between adjacent vias meet certain conditions. Various numerical techniques, such as mode-matching methods [17], finite-difference time domain [23], and T-matrix combining with lattice sums [24], [25], have been developed to accurately formulate the EM scattering from periodic structures. However, tedious programming tasks for these methods are usually required. With the help of EM simulators, the scattering characteristics of periodic structures can be approximately obtained by simulating a single unit cell with periodic boundary conditions, as used in [20], [21], and [23]. Nevertheless, the periodic via arrays of coupling windows in a multi-aperture SIW coupler usually have a larger via spacing. When a plane wave impinges on them, high-order propagating Floquet modes may be excited [26], which will seriously deteriorate the isolations and aggravate the coupler's performance. Therefore, a selection criterion for via spacing is necessary.

In [27], a simplified ray tracing approach is introduced to trace the propagation path of each ray and then quickly predict the coupling characteristics of SIW-based multi-aperture couplers. In this paper, our previous work has been expanded further. The fundamental principle using the ray tracing method is described in detail. The principal mode (TE_{10} mode) in SIWs is divided into two plane wave rays. Each ray can be effectively traced until they have reached the output ports. The transverse electrical field components for these rays at each reflection point are formulated successively. The output power at each output port is obtained by summing up the powers carried by all rays reaching that port. The detailed formulas are deduced that can be applied to calculate the coupling coefficients of SIW couplers with the transmission and reflection coefficients at the coupling window. The procedure to get the initial values of SIW couplers is given, and three examples are shown to validate the accuracy of our approach. It is known that the simplified ray tracing method can provide only approximate results. However, it is accurate enough to

Manuscript received June 9, 2016; revised September 11, 2016; accepted November 3, 2016. Date of publication December 16, 2016; date of current version January 10, 2017. Recommended for publication by Associate Editor M. S. Tong upon evaluation of reviewers' comments. *(Corresponding author: Zheng Liu.)*

The authors are with the Key Laboratory of Ministry of Education of Design and EM Compatibility of High Speed Electronic Systems, Shanghai Jiao Tong University, Shanghai 200240, China (e-mail: lzheng1984@163.com).

Color versions of one or more of the figures in this paper are available online at http://ieeexplore.ieee.org.

Digital Object Identifier 10.1109/TCPMT.2016.2626382

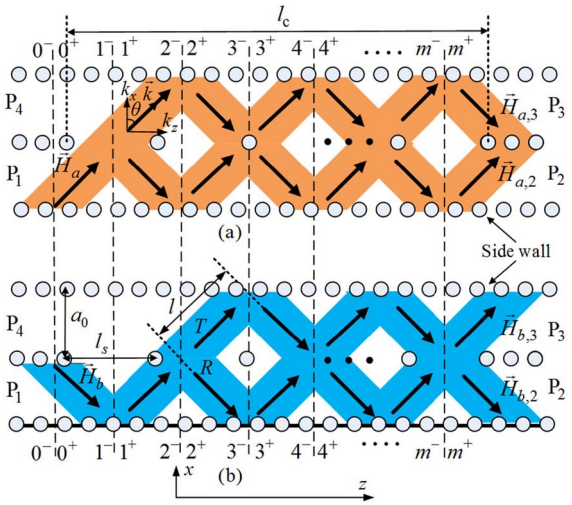

Fig. 1. Schematic for multi-aperture directional coupler with ray-tracing paths. (a) Wave ray a. (b) Wave ray b.

provide good initial values for geometrical parameters. The final optimization process with a commercial EM simulator will be greatly improved starting from these initial values. Furthermore, based on the Floquet theorem, a criterion for the via spacing in the coupling windows is derived to prevent exciting high-order propagating Floquet modes in the designed SIW-based couplers, which is critical to enhance the isolations among output ports.

This paper is organized as follows. The simplified ray tracing approach is described in Section II. In Section III, the Floquet theorem is used to deduce the criterion for via spacing. The design procedure for multi-aperture couplers is described in Section IV. Three examples of multiway coupler design are shown in Section V. Finally, a conclusion of this paper is given in Section VI. The time dependence $e^{-j\omega t}$ is assumed and omitted throughout this paper.

II. Ray Tracing Method

An SIW-based multi-aperture directional coupler is shown in Fig. 1. The two sidewalls can be equivalently modeled as perfect electrically conducting (PEC) walls in Fig. 1, from which all EM waves are totally reflected. The coupling window is composed of circular metallic vias that are placed periodically along the z-direction with a periodic distance of l_s, and its overall length is denoted by l_c. P_1, P_2, P_3, and P_4 represent the input, through, coupling, and isolation ports, respectively.

Assume that the only propagation mode is the principal mode, i.e., TE_{10} mode, which can be decomposed into two plane wave rays, denoted, respectively, by $\vec{H}_a$ and $\vec{H}_b$ in Fig. 1. Note that in the coordinate system shown in Fig. 1, the electric fields of the two rays have only the y-component and $E_{ya} = E_{yb}$ at the input port. The two wave rays propagate along the directions at angles $\pm\theta$ with respect to the x-axis [28]. The wavenumber is k. The width of each ray is $a_e \sin\theta$, where a_e is the equivalent width of the SIW, and can be obtained using [28, eq. (9)].

The ray tracing method, which has been employed in many planar and cubic structures [29]–[31], is used to determine the reflection points and predict the propagation path of each ray within the coupler. It is observed that each ray travels in the coupler by multiple reflections on the sidewalls and the coupling windows. The two rays may experience different path loss, and the powers carried by them may become different when they reach the output ports. The power carried by each ray at each output port is determined by superimposing the reflected and transmitted powers at the coupling window. The total output power of each port can be calculated by summing up the powers of these two rays.

It is important to note that unwanted high-order propagating Floquet modes may be possibly excited in the SIW couplers when a plane wave ray illuminates upon the coupling sections. Therefore, accurately calculating the power carried by each ray may become difficult unless some assumptions are made as follows.

1) The SIWs in the couplers are of the same width, and only the principal mode, that is, TE_{10} mode, is considered in the SIW structure.
2) The losses caused by the vias and the substrate are low, and hence, at any reflection point, the following formula can be approximately applied:

$$|R|^2 + |T|^2 \approx 1. \tag{1}$$

Here, denote, respectively, the reflection coefficient and the transmission coefficient of field components at the coupling window as R ($R = |R|\, e^{-j\phi_R}$) and T ($T = |T|\, e^{-j\phi_T}$).

Therefore, the transverse electrical field components of these rays at each reflection point can be formulated successively with the ray tracing method. Take the propagation traces of ray $\vec{H}_a$ as an example, and sequentially number the reflection points in the coupling window with $1, 2, \ldots, m$. The propagation distance of each ray between sidewalls and the adjacent coupling window is assumed as l, as shown in Fig.1(b), which is related to the incident angle θ and can be approximately expressed as [28], [32]

$$l = a_e / \cos\theta \tag{2}$$

$$\theta = \arccos\left(\frac{\pi}{a_e k}\right) = \arccos\left(\frac{v}{2a_e f}\right) \tag{3}$$

where v denotes the phase velocity in the SIWs. It is clear that ray $\vec{H}_a$ in Fig. 1(a) will break into two beams traveling to P_2 and P_3. Take the ray $\vec{H}_a$as an example, its transverse electric field E_{ya} at each reflection point in the upper and lower SIWs can be formulated in the following way.

1) For odd m, the reflection points lie on the coupling window

$$\begin{aligned} E^{m^+}_{ya,2} &= \left(\mathrm{TE}^{m^-}_{ya,3} + \mathrm{RE}^{m^-}_{ya,2}\right) \\ E^{m^+}_{ya,3} &= \left(\mathrm{RE}^{m^-}_{ya,3} + \mathrm{TE}^{m^-}_{ya,2}\right) \\ E^{m^-}_{ya,i} &= e^{-j(\pi+2\phi)} E^{(m-2)^+}_{ya,i}, \quad i = 2, 3 \end{aligned} \tag{4}$$

where $\phi_0 = \vec{k} \cdot \vec{l}$, representing the phase variation of the ray $\vec{H}_a$ from the sidewalls to its adjacent coupling window. The first subscript in $E^m_{ya,2}$ means the y-component of the electric field of the ray $\vec{H}_a$, the second one is the output port number, and the superscript is the number of

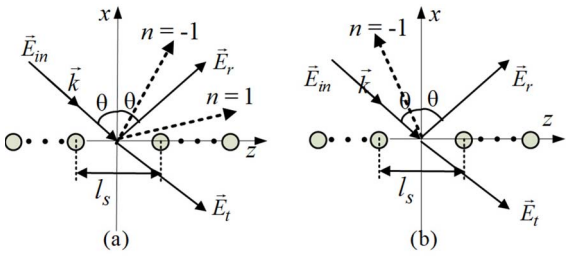

Fig. 2. (a) Possible high-order Floquet modes with $n = \pm 1$. (b) Lowest high-order Floquet mode with $n = -1$. Dashed lines mean the Floquet modes.

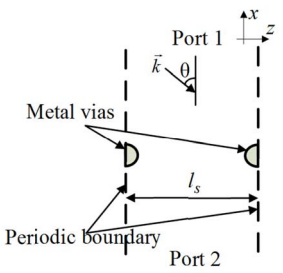

Fig. 3. Simulation model of a unit cell for coupling window.

reflection point. The upper scripts m^-/m^+ are applied to denote the fields just before/after the mth reflection point. Thus, at $m = 1$, we have $E^{1+}_{ya,2} = e^{-j\phi_0}\mathrm{RE}_a$ and $E^{1+}_{ay,3} = e^{-j\phi_0}\mathrm{TE}_a$.

2) For even m, the reflection points will lie on the sidewalls

$$\begin{aligned} E^{m+}_{ya,2} &= e^{-j\pi} E^{m-}_{ya,2} \\ &= e^{-j(\pi+2\phi)}\left(\mathrm{RE}^{(m-2)^+}_{ya,2} + \mathrm{TE}^{(m-2)^+}_{ya,3}\right) \\ E^{m+}_{ya,3} &= e^{-j\pi} E^{m-}_{ya,3} \\ &= e^{-j(\pi+2\phi)}\left(\mathrm{TE}^{(m-2)^+}_{ya,2} + \mathrm{RE}^{(m-2)^+}_{ya,3}\right). \end{aligned} \quad (5)$$

At $m = 0$, it can be found that $E^{0+}_{ya,2} = E_{ya}$, $|E^{0+}_{ya,3}| = 0$.

The electric fields of ray $\vec{H}_b$ at each reflection point can be obtained in the same way. Consequently, the coupling coefficients of this coupler at output ports can be explicitly calculated as follows:

$$\begin{aligned} D_{12} &= \left(\left|E^{m+}_{ya,2}\right|^2 + \left|E^{m+}_{yb,2}\right|^2\right) \Big/ |E|^2 \\ D_{13} &= \left(\left|H^{m+}_{a,3}\right|^2 + \left|H^{m+}_{b,3}\right|^2\right) \Big/ |E|^2. \end{aligned} \quad (6)$$

Note that with the simplified ray tracing method, no power comes out from the isolation port, i.e., P_4, in Fig. 1. Thus, the coupler is assumed to have an ideal isolation.

III. Criterion for the Via Spacing

From (4)–(6), the coupling coefficients D_{12} and D_{13} are mainly determined by the parameters of T, R, and m. For a fixed diameter of metallic via in the coupling window, the values of $T$and R are mainly determined by the via spacing l_s and the incidence angle θ. However, high-order propagating Floquet modes may be excited within the couplers when improper value of l_s is chosen [26], [28].

Consider an infinitely long periodic via array with via spacing l_s in the z-direction. It is illuminated by a TE plane wave with incident angle of θ with respect to the x-axis, as shown in Fig. 2(a). The wave vector of this incident wave is $\vec{k} = \hat{a}_z k\sin\theta - \hat{a}_x k\cos\theta$. According to the Floquet theorem [32], the scattered waves at both sides of the window can be expanded with Floquet modes, whose wave vectors can be expressed as $\vec{k}_n = \hat{a}_x k_{x,n} + \hat{a}_z k_{z,n}$, and

$$\begin{aligned} k_{z,n} &= k\sin\theta + (2n\pi)/l_s \\ k_{x,n} &= \sqrt{k^2 - k^2_{z,n}} \end{aligned} \quad (7)$$

where $k_{x,n}$ and $k_{z,n}$ are the propagation constants of the nth Floquet mode in the x- and z-direction, respectively. The zeroth-order mode ($n = 0$) corresponds to the reflected wave and the transmitted wave at the two sides of the coupling window.

High-order propagating Floquet modes will certainly convert power from the principal mode into high-order waveguide modes, which may cause higher insertion loss and deteriorate the isolation. It is evident that the lowest high-order Floquet mode is the mode associated with $n = -1$, as shown in Fig. 2(b). Therefore, in order to prevent the high-order modes from propagating, i.e., all high-order Floquet modes are evanescent waves, the following relation should be observed:

$$|k_{z,-1}| = |k\sin\theta - 2\pi/l_s| > k \quad (8)$$

from which the criterion for the via spacing can be deduced as

$$l_s < l_{s\max} = \frac{2\pi}{k + k\sin\theta} = \frac{v}{f\left[1 + \sqrt{1 - (v/2a_e f)^2}\right]} \quad (9)$$

The criterion (9) is based on infinitely long via array. In the cases of finite via arrays with n_a vias, their spectra are not discrete lines corresponding to Floquet modes anymore. Each spectral line will be blurred to cover a narrow spectrum band. However, for finite arrays with several periods, the relative frequency spread of the first Floquet mode is less than $1/n_a$, and the criterion in (9) is still approximately applicable. The criterion should be strictly satisfied in designing the coupling windows of SIW-based multi-aperture couplers. Under this criterion, the values of T and R for the coupling window can be quickly obtained by simulating its single unit cell model, as shown in Fig. 3, where periodic boundary conditions are assigned to the left and the right boundaries, and PEC walls are assigned to the front and the rear boundary. A y-polarized plane wave with incident angle θ is applied to the cell from the port 1. It can be proved that $|R| = |S_{11}|$ and $|T| = |S_{21}|$.The values of $|S_{11}|$ and $|S_{21}|$ can be quickly obtained with the EM simulator. It is worthwhile to note that the values of R and T are directly related with incident angle θ, which is frequency-dependent. Fig. 4(a) shows the maximum allowable via spacing $l_{s\max}$ for coupling windows.

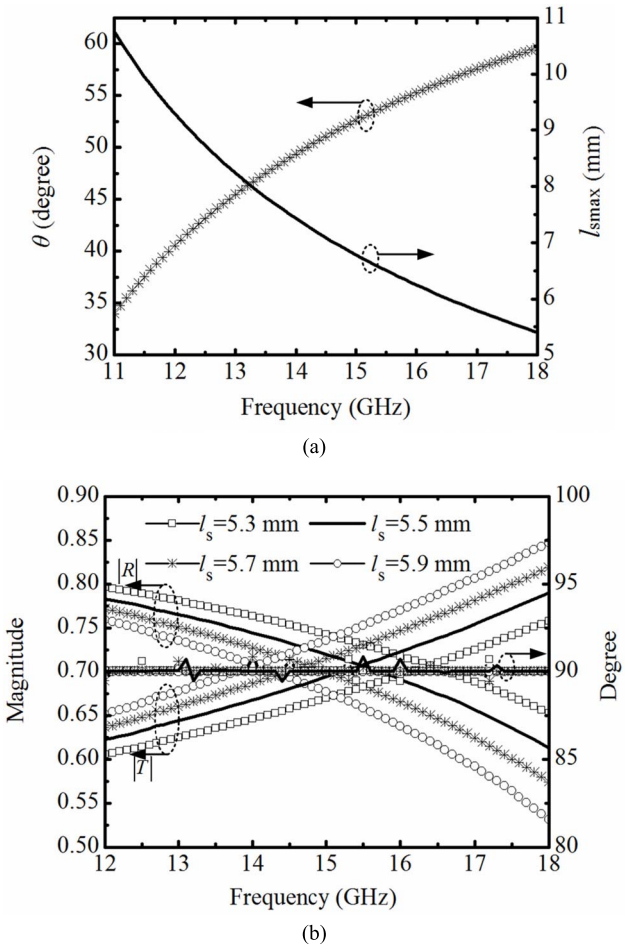

Fig. 4. (a) Incident angle θ and maximal via spacing $l_{s\,\max}$ versus frequency. (b) Magnitudes of R and T and the phase differences between R and T with different via spacings l_s (mm). The diameter of via is 1.0 mm.

Fig. 4(b) illustrates the simulated variation curves of the $|R|$ and $|T|$ and their phase differences for different via spacings l_s. If the ratio of via spacing to diameter is small, e.g., $l_s/d < 2.5$, the formulas for the transmission coefficient of coupling window given in [20] can be used, which is independent of frequency. Meanwhile, it is found that the phase differences between R and T are about $\pi/2$, which is almost independent of via spacing l_s.

IV. Design of Multi-Aperture Couplers

The ray tracing method is very simple to implement and very convenient to be used to create the prototype structures of SIW-based multi-aperture couplers with properly assigned initial values, starting from which the optimization efficiency can be greatly improved. The main design steps for SIW-based multi-aperture couplers are listed as follows.

1) Follow closed-form formulas [28], [33] to determine the dimensions of SIW and the sizes of transitions.
2) With formula (9), calculate the maximum via spacing $l_{s\,\max}$ associated with the upper boundary frequency f_H.
3) With parameters of the substrate, obtain the variation curves of T and R versus the via spacing l_s by simulating one unit of coupling window with periodic boundary conditions.
4) Derive the formulas of transverse electrical field components with (4) and (5) and then predict and analyze the power coupling coefficients with (6). Optimize the values of m and l_s until the power coupling coefficients meet the requirements at the center frequency first, and then balance its whole performance within its operating frequency band by fine-tuning their values. In this step, the optimization is fulfilled using the curves of R and T, together with the prediction formulas for the power division ratios like (4) and (5). It is not necessary to perform full-wave simulations.
5) Calculate the number of apertures n_a in the coupling window by

$$n_a = [ml \sin\theta_c / l_s] \tag{10}$$

where $[u]$ means taking the nearest integer of u and θ_c is the incidence angle expressed by (3) in the center frequency. Therefore, the coupling window consists of $(n_a + 1)$ vias. The prototype of the coupler is available.
6) Starting from the prototype and the initial values, optimize the whole SIW coupler with transitions using an EM simulator; usually, the first and last via spacings in the coupling section need to be slightly adjusted.

It is known that the ray tracing method can be further improved by dividing one ray into several parallel subrays. The coupling effect of the windows can be addressed more accurately with the subrays.

V. Experimental Verification

In this section, several examples are designed to verify the accuracy of the proposed approach. The substrate used in this paper is Taconic TLX with a thickness of 1 mm, a relative permittivity of 2.55, a relative permeability of 1.0, and a loss tangent of 0.0019. The diameter of the via is 1.0 mm, and the via spacing in the sidewalls is 1.8 mm in all the examples. The used EM software is HFSS 14.0.

A. Example of 3-dB Directional Coupler

A conventional 3-dB multi-aperture direction coupler is designed first to verify our proposed method. The traces of plane wave rays propagating within this coupler can be plotted, which have also been given in Fig. 1. Based on the criterion (9), the via spacing l_s is set as 5.5 mm to avoid high-order propagating Floquet modes within SIWs. First, the values of R and T are obtained with the EM simulator. Second, the transverse electric field components for ray $\vec{H}_a$ and $\vec{H}_b$ at P_2 and P_3 are formulated, respectively, for $m = 4$. Third, the coupling coefficients at output ports, i.e., D_{12} and D_{13}, can be predicted using the simplified ray tracing formulation, as illustrated in Fig. 5(b). Fourth, the number of apertures n_a in the coupling window is derived as 8 with (10). Finally, the entire layout of the designed directional coupler with transitions is optimized, fabricated, and measured. The phase balance between output ports can also be obtained from the formulas of transverse electrical field components.

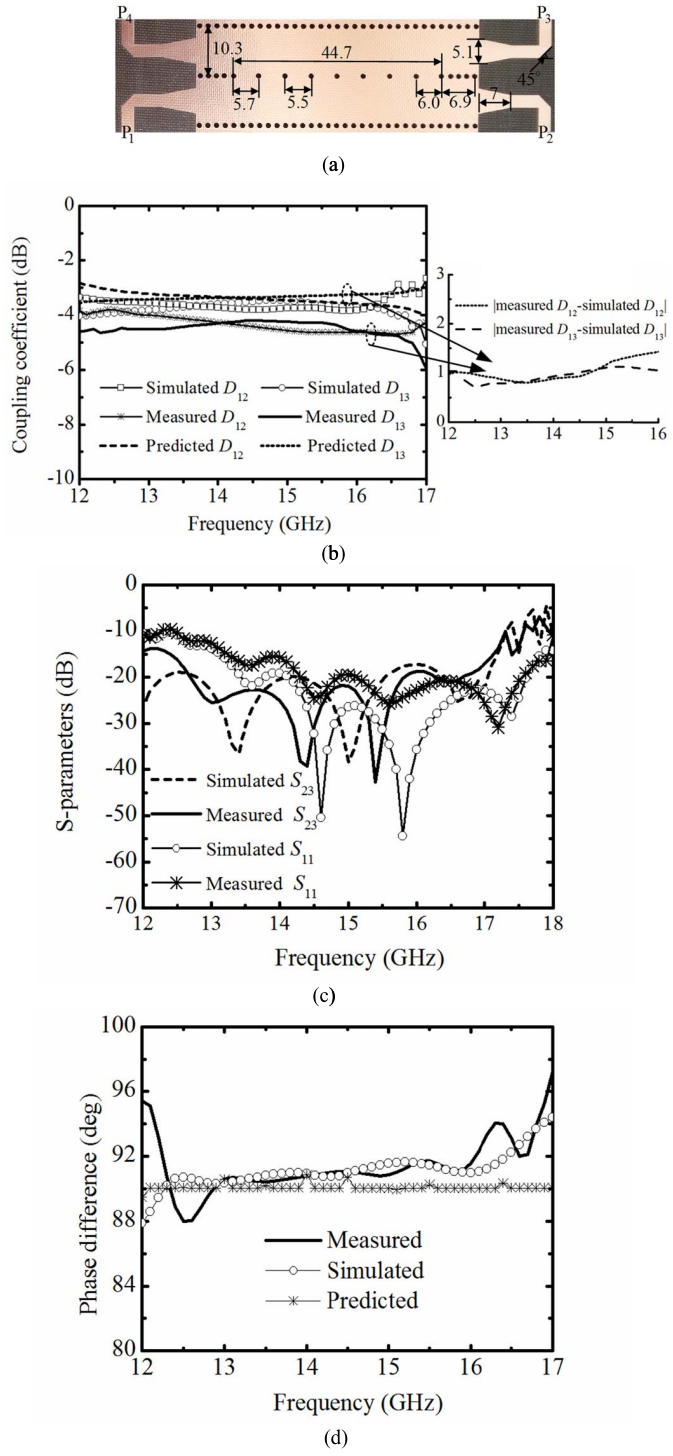

Fig. 5. (a) Photograph of the multi-aperture directional coupler (mm). Predicted, simulated, and measured scatter parameters of (b) coupling coefficients, (c) isolations, and (d) phase differences between P_2 and P_3.

Fig. 5(a) shows the photograph of the fabricated 3-dB coupler. The geometries after optimization have been marked in the photograph. The first via spacing in the coupling window has increased from its original value of 5.5–5.7 mm, and the last one varies from 5.5 to 6.0 mm, while other sizes remain unchanged. The simulated and measured scattering parameters are given in Fig. 5(b)–(d). Meanwhile, Table I lists the

TABLE I
RESULTS OF THE 3-dB DIRECTIONAL COUPLER

	Predicted	Simulated	Measured
D_{12} (dB)	3.2±0.5	3.6±0.5	4.3±0.5
D_{13} (dB)	3.3±0.5	3.5±0.5	4.2±0.5
S_{23} (dB)	∞	>17.5	>15
Phase difference for S_{23}(deg)	90±0.3	90±1.5	91±3
Bandwidth (GHz)	12.2∼17.0	12.2∼16.9	12.4∼17

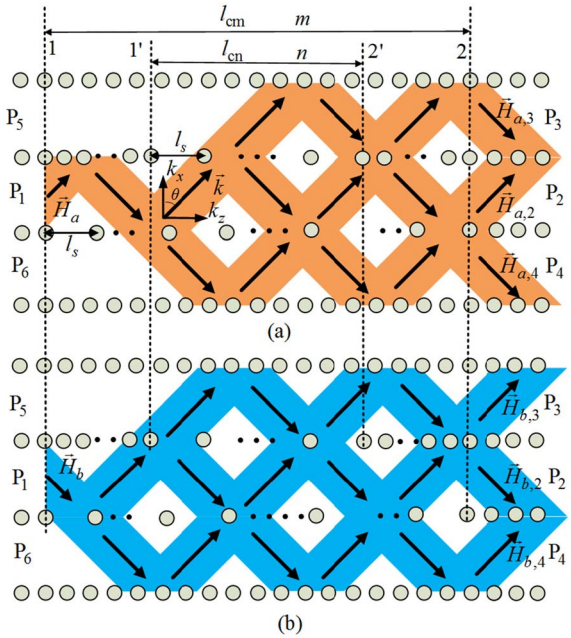

Fig. 6. Traces of rays within three-way coupler. (a) Ray a. (b) Ray b. l_{cm} and l_{cn} are the lengths of two coupling windows, respectively. m and n are, respectively, the number of the reflection points within the two coupling windows.

detailed comparison of the predicted, simulated, and measured results.

The predicted results have not taken into account factors such as losses caused by port discontinuities and the EM scattering effects. The measured results have included the contributions of the SMA connectors. From Table I, it can be found that the measured operating bandwidths of the coupling coefficients between output ports agree well with the simulated and predicted ones. Good isolations and phase balance among output ports are also observed. Meanwhile, the isolations begin to deteriorate at a frequency of 17.3 GHz in Fig. 5(c), which is close to the upper critical frequency ($f_H = 17.6$ GHz) at which the first propagating Floquet mode begins to appear. The designed 3-dB multi-aperture coupler has achieved a 31% relative operating bandwidth.

B. Three-Way Couplers With Equal/Unequal Power Division Ratio

In microwave and millimeter-wave communication systems and the antenna beamforming networks, multiway power dividers/couplers with equal and unequal power division ratios are usually required according to different application

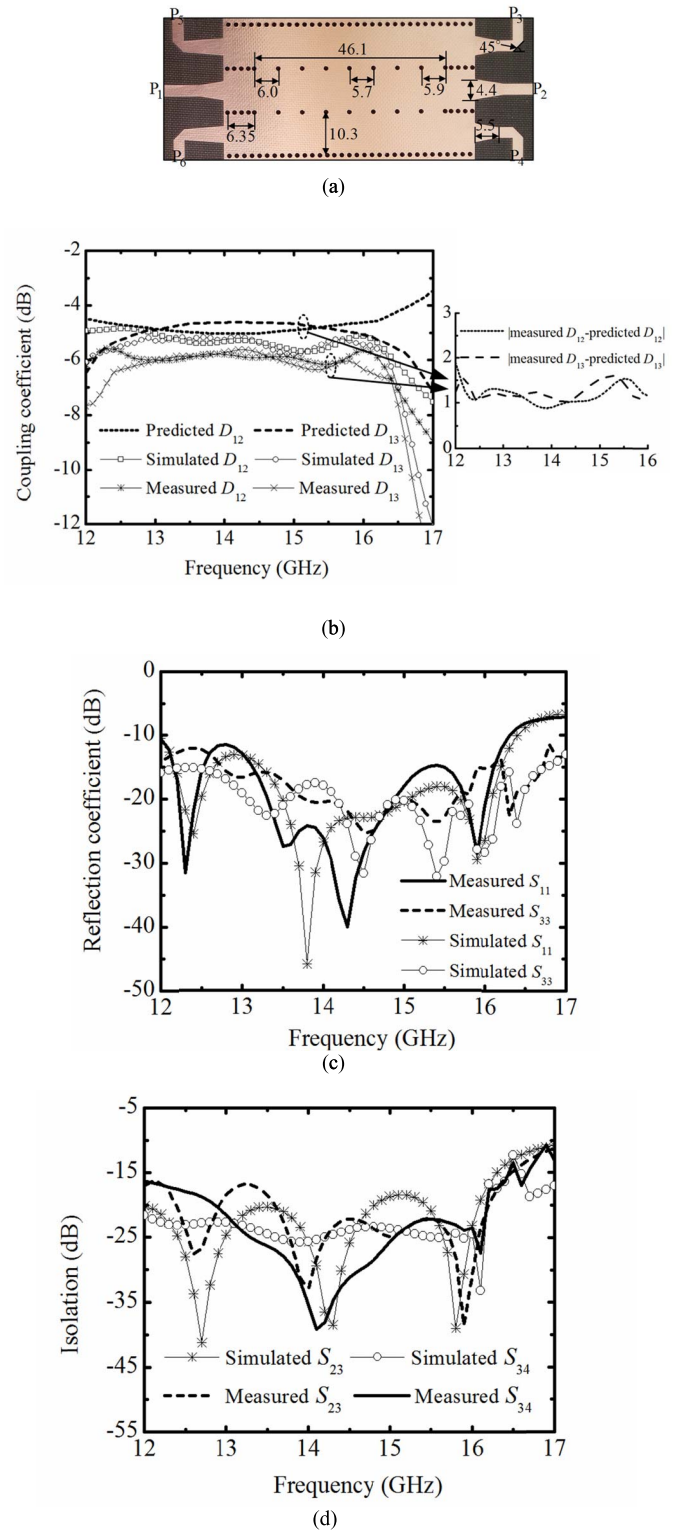

Fig. 7. (a) Photograph of fabricated three-way equiratio coupler (mm). (b)–(d) Comparison of the predicted, simulated, and measured scattering parameters.

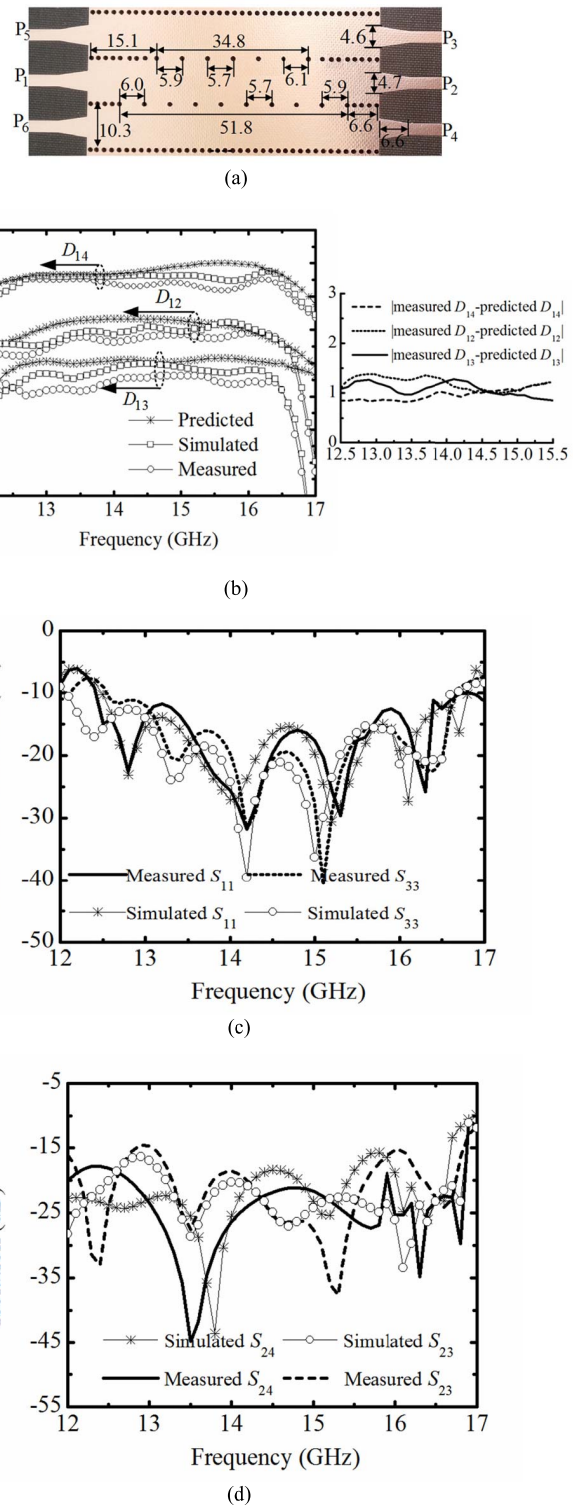

Fig. 8. (a) Photograph of fabricated three-way unequiratio coupler (mm). (b)–(d) Comparison of the predicted, simulated, and measured scattering parameters of unequal three-way coupler.

background [16], [17], [19]. In this section, two three-way couplers with equal/unequal power division ratios are designed to verify the accuracy of our approach further. The equiratio three-way coupler is realized with a uniform structure, which is symmetrical on its axial direction, and the two coupling windows have the same length ($l_{cn} = l_{cm}$ and $n = m$ in Fig. 6), while the unequal ratio one is designed with an unsymmetrical structure, in which the two coupling windows have different lengths ($l_{cn} \neq l_{cm}$ and $n \neq m$). Fig. 6 shows a model of the three-way multi-aperture coupler with an unequal power division ratio, together with the traces of wave rays

TABLE II
THREE-WAY COUPLER WITH EQUAL/UNEQUAL POWER DIVISION RATIO

EQUAL POWER DIVISION RATIO

	Predicted	Simulated	Measured
D_{12} (dB)	4.9±0.5	5.4±0.5	6.1±0.5
D_{13} & D_{14} (dB)	4.7±0.5	5.3±0.5	6.0±0.5
S_{23} & S_{24} (dB)	∞	>18	>16.5
S_{34} (dB)	∞	>22	>17
Bandwidth (GHz)	12.3～16.7	12.3～16.6	12.5～16.4

UNEQUAL POWER DIVISION RATIO

	Predicted	Simulated	Measured
D_{12} (dB)	5.8±0.5	6.3±0.5	7.0±0.5
D_{13} (dB)	8.2±0.5	8.8±0.5	9.4±0.5
D_{14} (dB)	2.3±0.5	2.8±0.5	3.3±0.5
S_{23} (dB)	∞	>18	>16
S_{24} (dB)	∞	>17.5	>15
Bandwidth (GHz)	12.2～16.6	12.2-16.5	12.5-16.3

within it. For the sake of convenience, the two coupling windows are assumed to have identical periodic distance of l_s. The operating frequency bands of the two couplers are the same, ranging from 12.5 to 16.5 GHz. According to Fig. 4(a), the value of l_s is set as 5.7 mm ($f_H = 17.1$ GHz) to get higher isolations and minimize their dimensions.

Similarly, the principal mode is also divided into $\vec{H}_a$ and $\vec{H}_b$ at a reference point near the left edge of the coupling windows, as shown in Fig. 6. In this case, these two rays will, respectively, break into three beams. Thus, the transverse electrical field components for each ray at output ports can be obtained sequentially with similar expressions as those in (4) and (5).

The couping ceofficients D_{12}, D_{13}, and D_{14} for the equiratio coupler can be calculated analogous to (6), and their curves have been shown in Fig. 7(b). The values of m and n_a are set as 5 and 8, respectively. Since D_{14} equals D_{13} for the equiratio coupler, only the curves of D_{13} and D_{12} are shown. In the similar way, the predicted coupling coefficients for the unequal ratio coupler are illustrated in Fig. 8(b). In this case, the values of m and n in Fig. 6 are set as 6 and 4, respectively, which correspond to the numbers of the apertures 9 and 6, respectively. Finally, the two couplers are all fabricated, and their photographs are shown in Figs.7(a) and 8(a), respectively.

It is noted that for these two couplers, the original value of via spacing in the coupling sections is 5.7 mm. When the whole circuit models including the transition parts are simulated and optimized, only the first and last via spacings in their coupling windows have been adjusted, while the other values will remain the same, as shown in Figs. 7(a) and 8(a), respectively. The simulated and measured results of these two couplers are, respectively, shown in Figs. 7(b)–(d) and 8(b)–(d). Good agreement is again observed among the measured results and those simulated and predicted ones of the two couplers. Good isolations among output ports have been achieved. Meanwhile, it is found that the measured isolations begin to deteriorate seriously when the frequency is beyond 16.8 GHz, which is close to the upper critical frequency ($f_H = 17.1$ GHz). Table II shows the predicted, simulated, and measured results of these two couplers.

VI. CONCLUSION

In this paper, a simplified method is applied to trace the wave rays in SIW-based multi-aperture couplers, and formulas to calculate the coupling coefficients of output ports are derived. Good initial values for the geometrical parameters of SIW-based multi-aperture couplers can be obtained quickly with the ray tracing method, with which the optimizing efficiency of the entire layout can be greatly improved. High isolation among output ports can be achieved by observing the criterion for via spacing in the coupling window. Several examples of SIW-based multi-aperture couplers are designed and fabricated, and the measured results verified the proposed approach.

REFERENCES

[1] M. Bozzi, A. Georgiadis, and K. Wu, "Review of substrate-integrated waveguide circuits and antennas," *Microw., Antennas Propag.*, vol. 5, no. 8, pp. 909–920, Jun. 2011.
[2] B. Y. El Khatib, T. Djerafi, and K. Wu, "Substrate-integrated waveguide vertical interconnects for 3-D integrated circuits," *IEEE Trans. Compon., Packag., Manuf. Technol.*, vol. 2, no. 9, pp. 1526–1535, Sep. 2012.
[3] K.-S. Chin, C.-C. Chang, C.-H. Chen, Z. Guo, D. Wang, and W. Che, "LTCC multilayered substrate-integrated waveguide filter with enhanced frequency selectivity for system-in-package applications," *IEEE Trans. Compon., Packag., Manuf. Technol.*, vol. 4, no. 4, pp. 664–672, Apr. 2014.
[4] X.-P. Chen and K. Wu, "Self-packaged millimeter-wave substrate integrated waveguide filter with asymmetric frequency response," *IEEE Trans. Compon., Packag., Manuf. Technol.*, vol. 2, no. 5, pp. 775–782, May 2012.
[5] Z. Liu, L. Zhu, G. Xiao, and Q. S. Wu, "An effective approach to deembed the complex propagation constant of half-mode SIW and its application," *IEEE Trans. Compon., Packag., Manuf. Technol.*, vol. 6, no. 1, pp. 109–116, Jan. 2016.
[6] H. Schmiedel and F. Arndt, "Field theory design of rectangular waveguide multiple-slot narrow-wall couplers," *IEEE Trans. Microw. Theory Techn.*, vol. 34, no. 7, pp. 791–798, Jul. 1986.
[7] A. Patrovsky, M. Daigle, and K. Wu, "Coupling mechanism in hybrid SIW–CPW forward couplers for millimeter-wave substrate integrated circuits," *IEEE Trans. Microw. Theory Techn.*, vol. 56, no. 11, pp. 2594–2601, Nov. 2008.
[8] B. Liu, W. Hong, Y.-Q. Wang, Q.-H. Lai, and K. Wu, "Half mode substrate integrated waveguide (HMSIW) 3-dB coupler," *IEEE Microw. Wireless Compon. Lett.*, vol. 17, no. 1, pp. 22–24, Jan. 2007.
[9] G. H. Zhai *et al.*, "Folded half mode substrate integrated waveguide 3 dB coupler," *IEEE Microw. Wireless Compon. Lett.*, vol. 18, no. 8, pp. 512–514, Aug. 2008.
[10] T. Djerafi, K. Wu, and S. O. Tatu, "3 dB 90° hybrid quasi-optical coupler with air field slab in SIW technology," *IEEE Microw. Wireless Compon. Lett.*, vol. 24, no. 4, pp. 221–223, Apr. 2014.
[11] M. Kishihara, M. Komatsubara, K. Okubo, and I. Ohta, "Broadband cruciform substrate integrated waveguide couplers," in *Proc. Asia–Pacific Microw. Conf.*, Singapore, Dec. 2009, pp. 2100–2103.
[12] P.-L. Chi and T.-Y. Chen, "Dual-band ring coupler based on the composite right/left-handed folded substrate-integrated waveguide," *IEEE Microw. Wireless Compon. Lett.*, vol. 24, no. 5, pp. 330–332, May 2014.
[13] X. Zou, C.-M. Tong, C.-Z. Li, and W.-J. Pang, "Wideband hybrid ring coupler based on half-mode substrate integrated waveguide," *IEEE Microw. Wireless Compon. Lett.*, vol. 24, no. 9, pp. 596–598, Sep. 2014.
[14] A. Doghri, T. Djerafi, A. Ghiotto, and K. Wu, "Substrate integrated waveguide directional couplers for compact three-dimensional integrated circuits," *IEEE Trans. Microw. Theory Techn.*, vol. 63, no. 1, pp. 209–221, Jan. 2015.
[15] S. E. Miller and W. W. Mumford, "Multi-element directional couplers," *Proc. IRE*, vol. 40, no. 9, pp. 1071–1078, Sep. 1952.

[16] Z. Liu and G. Xiao, "New multi-way SIW power dividers with high isolation," in *Proc. Asia–Pacific Microw. Conf.*, Sendai, Japan, Nov. 2014, pp. 702–704.
[17] Z. Kordiboroujeni, J. Bornemann, and T. Sieverding, "Mode-matching design of substrate-integrated waveguide couplers," in *Proc. Asia–Pacific Symp. Electromagn. Compat. (APEMC)*, Singapore, May 2012, pp. 701–705.
[18] D. Dousset, J. Bornemann, M. Daigle, S. Claude, and K. Wu, "Broadband 100 GHz Substrate-Integrated Waveguide couplers with irregularly shaped via holes for higher-order mode suppression," in *Proc. Eur. Microw. Conf.*, Amsterdam, The Netherlands, Nov. 2012, pp. 277–280.
[19] M. Pasian, M. Bozzi, and L. Perregrini, "Radiation losses in substrate integrated waveguides: A semi-analytical approach for a quantitative determination," in *IEEE MTT-S Int. Microw. Symp. Dig.*, Seattle, WA, USA, Jun. 2013, pp. 1–3.
[20] M. Pasian, M. Bozzi, and L. Perregrini, "A formula for radiation loss in substrate integrated waveguide," *IEEE Trans. Microw. Theory Techn.*, vol. 62, no. 10, pp. 2205–2213, Oct. 2014.
[21] M. Pasian, M. Bozzi, and L. Perregrini, "Crosstalk in substrate integrated waveguides," *IEEE Trans. Electromagn. Compat.*, vol. 57, no. 1, pp. 80–86, Feb. 2015.
[22] N. Marcuvitz, *Waveguide Handbook*. New York, NY, USA: Peregrinus, 1951.
[23] A. Alexanian, N. J. Kolias, R. C. Compton, and R. A. York, "Three-dimensional FDTD analysis of quasi-optical arrays using Floquet boundary conditions and Berenger's PML," *IEEE Microw. Guided Wave Lett.*, vol. 6, no. 3, pp. 138–140, Mar. 1996.
[24] A. Zeid and H. Baudrand, "Electromagnetic scattering by metallic holes and its applications in microwave circuit design," *IEEE Trans. Microw. Theory Techn.*, vol. 50, no. 4, pp. 1198–1206, Apr. 2005.
[25] J. Yang, L.-W. Li, K. Yasumoto, and C.-H. Liang, "Two-dimensional scattering of a Gaussian beam by a periodic array of circular cylinders," *IEEE Trans. Geosci. Remote Sens.*, vol. 43, no. 2, pp. 280–285, Feb. 2002.
[26] Y. Tan, Z. Hu, B. Zhu, and L. Zhou, "Scattering characteristics of dielectric periodic structures based on Floquet mode analysis and hybrid finite element methods," in *Proc. 5th Global Symp. Millim. Waves*, Harbin, China, May 2012, pp. 174–177.
[27] Z. Liu, G. Xiao, and J. Mao, "An approximate method to predict the characteristics of SIW-based directional coupler," in *Proc. IEEE 4th Asia–Pacific Conf. Antennas Propag. (APCAP)*, Jun./Jul. 2015, pp. 529–530.
[28] F. Xu and K. Wu, "Guided-wave and leakage characteristics of substrate integrated waveguide," *IEEE Trans. Microw. Theory Techn.*, vol. 53, no. 1, pp. 66–73, Jan. 2005.
[29] S. Y. Seidel and T. S. Rappaport, "Site-specific propagation prediction for wireless in-building personal communication system design," *IEEE Trans. Veh. Technol.*, vol. 43, no. 4, pp. 879–891, Nov. 1994.
[30] C.-F. Yang, B.-C. Wu, and C.-J. Ko, "A ray-tracing method for modeling indoor wave propagation and penetration," *IEEE Trans. Antennas Propag.*, vol. 46, no. 6, pp. 907–919, Jun. 1998.
[31] B. A. Munk, *Frequency Selective Surfaces: Theory and Design*. New York, NY, USA: Wiley, 2000.
[32] D. M. Pozar, *Microwave Engineering*. 4th ed. Hoboken, NJ, USA: Wiley, Nov. 2012.
[33] D. Deslandes and K. Wu, "Integrated microstrip and rectangular waveguide in planar form," *IEEE Microw. Wireless Compon. Lett.*, vol. 11, no. 2, pp. 68–70, Feb. 2001.

Zheng Liu (S'12) was born in Shandong, China, in 1984. He is currently pursuing the Ph.D. degree with Shanghai Jiaotong University, Shanghai, China.

He was an Exchange Student from the University of Macau, Macau, China, from 2014 to 2015. His current research interests include microwave and millimeter-wave passive and active components and circuits.

Gaobiao Xiao (M'09) received the B.S. degree from the Huazhong University of Science and Technology, Wuhan, China, in 1988, the M.S. degree from the National University of Defense Technology, Changsha, China, in 1991, and the Ph.D. degree from Chiba University, Chiba, Japan, in 2002.

He was with Hunan University, Changsha, from 1991 to 1997. He has been a Faculty Member with the Department of Electronic Engineering, Shanghai Jiao Tong University, Shanghai, China, since 2004. His current research interests include numerical methods in electromagnetic fields, coupled thermoelectromagnetic analysis, microwave filter designs, fiber-optic filter designs, and inverse scattering problems.